



Research on the unusual spring 2020 Arctic stratospheric ozone depletion above Ny-Ålesund, Norway

Qidi Li^{1,2}, Yuhan Luo^{1*}, Yuanyuan Qian^{1,2}, Chen Pan^{3,4}, Ke Dou¹, Xuewei Hou⁵, Fuqi Si¹, Wenqing Liu¹

5 ¹Key Laboratory of Environmental Optics and Technology, Anhui Institute of Optics and Fine Mechanics, Hefei Institutes of Physical Science, Chinese Academy of Sciences, Hefei, 230031, China

²University of Science and Technology of China, Hefei, 230026, China

³Jiangsu Meteorological Observatory, Jiangsu Meteorological Bureau, Nanjing, 210008, China

⁴Key Laboratory of Transportation Meteorology, China Meteorological Administration, Nanjing, 210009, China

10 ⁵Collaborative Innovation Center on Forecast and Evaluation of Meteorological Disasters, Nanjing University of Information Science and Technology, Nanjing, 210044, China

Correspondence to: Yuhan Luo (yhluo@aiofm.ac.cn)

Abstract. Of the severe stratospheric ozone depletion events (ODEs) reported over the Arctic, the third and most severe occurred during the spring of 2020; we analyzed the reasons for this event herein. We retrieved the critical indicator ozone vertical column density (VCD) using zenith scattered light differential optical absorption spectroscopy (ZSL-DOAS) located in Ny-Ålesund, Svalbard, Norway. The average ozone VCDs over Ny-Ålesund between March 18 and April 18, 2020, were approximately 274.8 Dobson units (DU), which was only 64.7% of that in normal years. The retrieved daily averages of ozone VCDs were compared with satellite observations from Global Ozone Monitoring Experiment 2 (GOME-2), a Brewer spectrophotometer, and a Système d'Analyse par Observation Zénithale (SAOZ) spectrometer at Ny-Ålesund; the resulting Pearson correlation coefficients were relatively high at 0.94, 0.86, and 0.91, with relative deviations of 2.3%, 3.1%, and 3.5%, respectively. Compared with normal years, the 2020 daily peak relative ozone loss was 44.3%. During the 2020 Arctic spring ODE, the ozone VCDs and potential vorticity (PV) had a negative correlation with their fluctuations, suggesting a clear effect of the polar vortex on stratospheric ozone depletion. To better understand what caused the ozone depletion, we also considered the chemical components of this process in the Arctic winter of 2019/2020 with the specified dynamics version of the Whole Atmosphere Community Climate Model (SD-WACCM). The SD-WACCM results indicated that both CIO and BrO concentrations peaked in late March, which was a critical factor during the ozone depletion observed in Ny-Ålesund. Chlorine activation was clearly apparent during the Arctic spring of 2020, whereas the partitioning of bromine compounds was different from that of chlorine. By combining observations with modeling, we provide a reliable basis for

25



further research on global climate change due to polar ozone concentrations and the prediction of severe Arctic ozone
30 depletion in the future.

Key Words: Arctic ozone depletion, DOAS, ozone VCD, polar vortex, SD-WACCM, halogen species

1 Introduction

Stratospheric ozone is essential for human health, surface ecosystems, and the climate in general (McKenzie et al., 2011)
because it absorbs ultraviolet (UV) solar radiation and converts it into thermal energy. The characteristic absorption bands of
35 stratospheric ozone are mainly located in the Hartley and Huggins zones of the UV region and in the Chappuis zone of the
visible spectrum, thereby absorbing almost all UV-C (i.e., wavelengths < 280 nm) and some UV-B (i.e., wavelengths
ranging between 280 and 315 nm) radiation. Since the late 1970s, Antarctic stratospheric ozone during the austral spring has
decreased sharply, mainly because of the heterogeneous catalytic reactions between ozone and active halogen radicals
generated by the conversion of chlorofluorocarbons derived from anthropogenic emissions (Farman et al., 1985). As
40 anthropogenic emissions of ozone-depleting substances since the Montreal Protocol was enforced, the concentrations of
ozone in the stratosphere were predicted to recover to pre-1980 values in 2060 (Solomon et al., 2016).

The severe ozone depletion over the Arctic is relatively uncommon compared with that in the Antarctic. During normal
Arctic winters, the polar vortex usually fractures and disperses early due to huge planetary wave activities and Brewer–
Dobson circulation dynamics (Manney et al., 2003; Dameris, 2010; Harris et al., 2010). Thus, in the Arctic, the duration of
45 the vortex is shorter and relative ozone loss is also lower (Solomon et al., 2007). However, irregular changes in Arctic ozone
in recent years have attracted worldwide attention and challenged the existing model. The most severe Arctic ozone
depletion lasted for nearly a month, from March to April 2020 (Dameris et al., 2021). Between mid-February and late March
2020, the persistence of anomalously faint wave activities in the Arctic led to an abnormally persistent and cold vortex,
which caused significant ozone loss (Hu, 2020). This event was the third reported low Arctic ozone event, following those
50 that occurred in the springs of 1997 and 2011 (Hansen and Chipperfield, 1999; Manney et al., 2011).

The powerful and persistent vortex during the winter and spring is considered a main cause of significant ozone depletion in
the Arctic (Bognar et al., 2021). Extremely low air temperatures (< -195 K) are essential to produce polar stratospheric



clouds (PSC). The PSC formed from water-ice and nitric acid trihydrate can be used as a surface for heterogeneous interactions, leading to the conversion of reactive halogens from the halogen reservoirs, which can cause serious ozone loss (Frieß et al., 2005; Marsing et al., 2019). PSCs are classified into three types: nitric acid trihydrate (NAT), ice PSCs, and supercooled ternary solution (STS), and their threshold temperatures are T_{nat} (−195 K), T_{ice} , and T_{sts} , respectively (Toohey et al., 1993). PSC might also grow large enough to precipitate and remove HNO_3 in the stratosphere, which is the reservoir of NO_2 . The resulting denitrification from the polar vortex hinders chlorine deactivation by NO_2 (Salawitch et al., 1989; Arblaster et al. 2014). Active chlorine is rapidly photolyzed because of the recovery of spring sunlight when ozone loss occurs via the self-reaction of ClO (Molina and Molina, 1987), as well as the cross-reaction of ClO and BrO (McElroy et al., 1986). It is essential that the vortex retains low temperatures and carries on as a transport impediment so that ozone can remain depleted without NO_2 to inactivate chlorine.

The observed Arctic ozone depletion is invaluable for validating stratospheric ozone simulations and for understanding the processes that cause Arctic stratospheric ozone depletion. Currently, total column ozone (TCO) detection utilizes the characteristic ozone absorption in the UV and visible spectra, which provides accurate ozone identification and quantitative measurements. Ozone vertical column density (VCD) is primarily achieved by satellite observation, Pandora spectrophotometer, Fourier-transform infrared spectrometer, Brewer spectrophotometer, balloon-borne ozone sonde, and ground-based differential optical absorption spectroscopy (DOAS) observation (Kuttippurath et al., 2012; Manney et al., 2020; Bogner et al., 2021; Groß and Müller, 2021). Among these, ground-based observations are crucial to calibrate remotely sensed observations and optimizing inversion results (Lu et al., 2006). The impacts of the aberrantly powerful and persistent vortex on ozone in the Arctic were investigated using satellite observations, ozonsonde measurements, and data from the European Centre for Medium-Range Weather Forecasts (ECMWF) (Wohlmann et al., 2020; Lawrence et al., 2020). The major stratospheric halogen species, chlorine, and bromine were investigated in this ozone depletion event (ODE) (Wohlmann et al., 2017, 2021). In addition, modeling plays an essential role in the investigation of ozone depletion (Simpson et al., 2007). Recently, stratospheric chemical patterns, consisting of a group of heterogeneous reactions, have been developed in various models according to investigations and experiments conducted in the polar area (McKenna et al., 2002; Groß et al., 2011, 2018). Global and area models using different stratospheric chemical patterns have been applied to



simulate ozone columns, which usually compare well with satellite observations and ozonsonde data (Pan et al., 2018; Grooß and Müller, 2021).

80 Accurate ground-based observations can make a significant impact on improving the accuracy and reliability of models as well as enhancing our understanding of the reasons for ozone depletion. We have developed a ground-based DOAS system that can conduct TCO observations in the Arctic. The zenith scattered light observation mode was applied to measure TCO using the Langley Plot method (Frieß et al., 2005).

We analyze the reasons for this ODE in the unusual spring of 2020 above Ny-Ålesund, Norway. The methods and data are
85 given in Sect. 2, which covers the presentation of the experimental location and DOAS instrument, the DOAS method, the specified dynamics version of the Whole Atmosphere Community Climate Model (SD-WACCM), Global Ozone Monitoring Experiment 2 (GOME-2) observations, Brewer measurements, Système d'Analyse par Observation Zénithale (SAOZ) measurements, ECMWF data, and ozonsonde data. Section 3 presents the results, where Sect. 3.1 describes the results of ozone VCDs from February 2017 to October 2021 and ozone loss in spring 2020. The zenith scattered light DOAS (ZSL-
90 DOAS) retrieved the daily variations in ozone VCDs, which were in comparison with GOME-2 observations, Brewer, and SAOZ measurements. A detailed characterization of this ODE is presented for establishing the basis of the subsequent analysis. The relationship between Arctic ozone depletion and meteorological conditions in terms to temperature and potential vorticity (PV) is described in Sect. 3.2. The effect of PV on ozone depletion was investigated using ozone VCD and stratospheric PV data. In Sect. 3.3, this ODE was analyzed using the SD-WACCM to further illustrate the ozone depletion
95 process, and to explore the effects of chemical depletion and dynamic transport on this ODE. The influence of the halogen species is discussed in Sect. 3.4. The comprehensive summary is provided in Sect. 4.

2 Methods

2.1 Experimental location and DOAS instrument

The DOAS instrument was placed at the Yellow River Station (78.92° N, 11.93° E) in the Arctic. Figure 1 shows the
100 experimental location and DOAS instrument, in Ny-Ålesund, Svalbard, Norway. The DOAS instrument mainly includes the prism, telescope, computer, and spectrometer. This spectrometer was designed for wavelengths between 290 and 420 nm,



and had the spectral resolution (FWHM) of 0.5 nm. The ozone slant column density (SCD) was retrieved, with the raw data obtained in the zenith direction.

2.2 Calculation of ozone VCD

105 Radiation intensity decreases when it passes through absorbing media (mainly trace gases). Because of the different absorption bands, characteristic peaks, and intensities of various gases, we can retrieve the content of each trace gas, according to Lambert–Beer’s law as follows:

$$\ln \frac{I^*(\lambda)}{I_0(\lambda)} = \sum[\sigma_j^*(\lambda)c_jL] = \sum[\sigma_j^*(\lambda)SCD_j]. \quad (1)$$

Here, $I_0(\lambda)$ represents the raw intensity of solar scattered spectral radiation received by the ground-based detector, $I^*(\lambda)$ denotes the incident intensity of the solar radiation spectrum, L represents the distance travelled by the incident light in the absorbing gas, $\sigma_j^*(\lambda)$ represents the absorption cross section for the j th gas, c_j denotes concentration of the j th gas, $SCD_j = \int c_jL$ represents the SCD of the j th gas, and $D = \ln \frac{I^*(\lambda)}{I_0(\lambda)}$ denotes the differential optical density.

We calculated the SCD for ozone with the QDOAS program (Platt and Stutz, 2008). In the experiment, ozone was retrieved in the 320–340 nm band, and the gases involved in the retrieval include O₃ (223K, 243K), NO₂ (298K), O₄ (293K), and ring
115 structure. Table 1 lists the parameters for the gases involved in the retrieval. Figure 2 shows a spectrum obtained during monitoring on June 13, 2021. The measured spectrum was fitted to give an ozone SCD of 4.09×10^{17} molec cm⁻², and the root mean square of the spectral fitting residual was 5.28×10^{-4} .

As SCD is dependent on the instrument's observation mode and the prevailing meteorological conditions, it is necessary to shift to VCD, which is independent of the mode of observation:

$$120 \quad AMF = \frac{SCD}{VCD}. \quad (2)$$

Here, the Air Mass Factor (AMF) can be obtained from the SCIATRAN model and is influenced by trace gas profiles, pressure, temperature, ozone, aerosol profiles, clouds, and surface albedo. Since the "Ring effect" in the measurement caused by the Fraunhofer reference spectra can lead to lower trace gas levels in the retrieval than in actual atmospheric levels, this is corrected in the calculation:

$$125 \quad dSCD(\alpha, \beta) = SCD(\alpha, \beta) - SCD_{FRS} = AMF(\alpha, \beta)VCD - SCD_{FRS}. \quad (3)$$



Here, SCD_{FRS} denotes Fraunhofer absorption. Figure 3 presents the results of a linear fit of the dSCD and AMF on June 13, 2021. The ozone VCD for this date was 8.799×10^{18} molec cm^{-2} and produced a fitting error of 3.361×10^{16} molec cm^{-2} . The uncertainties in ozone VCD retrieval originate from uncertainties in the retrieval of SCD and AMF. The error in retrieving ozone SCD was calculated as 3.01% within the 95% confidence interval. The solar zenith angle calculated in this research ranged between 35° and 80° , with surface albedos between 0.08 and 0.6. Based on the average monthly climate, *a priori* ozone profile can be achieved. Table 2 provides the parameters used to calculate the AMF effect on wavelength. The uncertainties of the AMF due to wavelength selection were calculated as $(AMF_\lambda - AMF_{328})/AMF_\lambda$, where λ denotes the wavelength. According to Table 2, the uncertainties of the AMF in the wavelength ranged from -4.257% to 4.630% , and the average uncertainty was 2.030%. Based on evaluation of the OMI ozone products, AMF had an uncertainty of about 2% for *a priori* ozone profile (Bhartia, 2002). The average AMF uncertainty was calculated as 2.85% using the following equation:

$\sqrt{AMF_{wave}^2 + AMF_{profile}^2}$, where AMF_{wave} denotes the error of AMF influenced by wavelength, and $AMF_{profile}$ denotes the AMF error affected through *a priori* ozone profile. The total error in the retrieved ozone VCD was 4.15%, calculated using the following error equation, $E_{VCD} = \sqrt{E_{SCD}^2 + E_{AMF}^2}$, where E_{SCD} and E_{AMF} denote the errors of SCD and AMF, respectively.

2.3 SD-WACCM

The parameters employed in the Community Atmosphere Model Version 4 (CAM4) were applied to the WACCM (Neale et al., 2013). We used the SD-WACCM with meteorological parameters driven by Modern Era Retrospective-Analysis for Research and Applications version 2 (MERRA-2) data (Gelaro et al., 2017). The Model for Ozone and Related Chemical Tracers, version 3 (MOZART-3) provided the chemical parameters for the WACCM (Kinnison et al., 2007). The SD-WACCM had the horizontal resolution of $1.9^\circ \times 2.5^\circ$ (lat \times lon). The model was divided vertically into 88 layers, covering an altitude of ~ 140 km from the ground to the bottom of the thermogenic layer. Meteorological fields were calculated using a nudging method in the model (Lamarque et al., 2012). Data from MERRA-2 guaranteed the accuracy of simulated values for meteorological fields below 50 km (Kunz et al., 2011). This can be employed for the study of specific weather events. Linear transitions were used in the 50–60 km altitude range and over 60 km, and online calculations were performed. The SD-



WACCM can be applied for research on chemical and dynamic processes in the atmosphere. (Lamarque et al., 2012; Pan et
150 al., 2019).

2.4 Auxiliary data

On October 19, 2006, Europe launched the MetOp-A satellite, which carries the GOME-2. The GOME-2 has a band between
240 and 790 nm, a spectral resolution ranging from 0.2 to 0.5 nm, and a nominal swath width spatial resolution of 80×40
km² (Koukouli et al., 2014). The GOME-2 dataset provided the daily mean VCD data (source: <https://avdc.gsfc.nasa.gov/>,
155 last access: 18 June 2022). Brewer spectrophotometers used holographic diffraction gratings to obtain the directly
transmitted intensity of sunlight. (Kerr, 2002). Ozone columns were calculated by averaging five consecutive measurements.
The error of the Brewer instrument was approximately 0.5% (Zhao et al., 2021). The Brewer dataset provided the daily mean
ozone data (source: <https://woudc.org/>, last access: 18 June 2022). The SAOZ instrument is a UV-Vis spectrometer
belonging to the worldwide analogous instrument networks (Pommereau and Goutail, 1988). The SAOZ instrument provided
160 a viewing angle of approximately 20° and measured trace gas concentrations in the stratosphere based on DOAS technology
(Platt & Stutz, 2008). Hendrick et al. calculated an error of 5.9% for the measurement of ozone by SAOZ (2011). The SAOZ
dataset provided the daily mean ozone VCD data (source: <http://saoz.obs.uvsq.fr/>, last access: 18 June 2022).

The ERA5 hourly pressure-levels data from 1959 to 2022 from the ECMWF website (source:
<https://www.ecmwf.int/en/newsletter/147/news/era5-reanalysis-production>, last access: 18 June 2022) provided the daily
165 temperature and PV data. ERA5 replaced ERA-Interim reanalysis. The ERA5 data have the spatial resolution of $0.25^\circ \times 0.25^\circ$
and were divided into 37 layers vertically, from 1000 hPa to 1 hPa. Since 1992, the Alfred Wegener Institute has recorded
the total ozone column and vertical profile using balloon-borne ozonesonde. The temporal resolution of the sounding data
from March 25 to April 13, 2020, is once per day, whereas the others are normally once per 3 d during the spring and once
per week during the other seasons (source: <https://ndaccdemo.org/>, last access: 12 January 2021).



170 **3 Results and discussion**

3.1 Results of ozone VCDs

The ozone VCDs obtained from the GOME-2 satellite, Brewer, SAOZ, and ground-based instruments from February 2017 to October 2021 are shown in Fig. 4. In normal years, ozone VCD begins to decrease in March and has a gradient of approximately 0.92 DU per day, while the lowest ozone VCDs occur in October. The average ozone VCD between March
175 18 and April 18, 2020, was at an abnormally low level of ~274.8 DU, with a minimum of 241.2 DU on April 5. The average ozone VCD during the same period in normal years was approximately 424.6 DU. All instruments detected relatively low levels of ozone from March 18 to April 18, 2020.

Figure 5 presents the linear fit between observed ozone VCDs and GOME-2 observations, Brewer, and SAOZ measurements. Their Pearson correlation coefficients were relatively high at 0.94, 0.86, and 0.91, and the relative deviations were 2.3%,
180 3.1%, and 3.5%, respectively. The ground-based DOAS measurements correlated well with ozone VCDs observed using GOME-2 onboard the MetOp satellite and Brewer and SAOZ instruments. Thus, the method of observing the VCDs of Arctic ozone using a ground-based DOAS instrument is reliable and valid.

The ozone data for 2020 and the average ozone data for the other years (2017, 2018, 2019, and 2021) from the ZSL-DOAS instrument, satellite observations from GOME-2, and measurements from the Brewer and SAOZ instruments are shown in
185 Fig. 6a. The diurnal means of absolute and relative ozone loss between data in 2020 and the mean of the other four years are displayed in Fig. 6b and Fig. 6c, respectively. In 2020, the daily peak absolute losses from the GOME-2, ZSL-DOAS, Brewer, and SAOZ datasets were 189.8, 195.7, 181.4, and 177.7 DU, respectively. The 2020 daily peak relative losses from the GOME-2, ZSL-DOAS, Brewer, and SAOZ datasets were 43.6%, 44.3%, 40.3%, and 40.6%, respectively.

3.2 Relation of Arctic ozone depletion to meteorological conditions

190 Daily average temperatures of Ny-Ålesund between November 2016 and September 2021 were measured at 70 hPa in the low stratosphere, where significant ozone depletion tends to occur (Fig. 7). Furthermore, temperatures dropped below the threshold (−195 K) at which the PSCs were formed. A relatively colder stratosphere over Ny-Ålesund persisted for a longer duration during the winter of 2019/2020 than in previous years, with air temperatures as low as 190 K. The number of days with daily temperatures below 195 K during the winters of 2017/2018, 2019/2020, and 2020/2021 are shown in Table 3. In



195 addition, overall winter temperatures in 2019/2020 were lower than those of the same period in normal years and had a prolonged period with cool temperature, leading to prolonged PSCs. Because of the atypically faint wave activities that occurred between mid-February and late March 2020 over the Northern Hemisphere (Dameris et al., 2021), the trend for abrupt warming in spring 2020 was lower than in normal years.

Ozone depletion occurs when the temperature is sufficiently low and reaches a threshold temperature. In addition, a cold and
200 stable polar vortex is a prerequisite for ensuring that Arctic stratospheric temperatures are sufficiently low. The sign of PV was positive in the Arctic and negative in Antarctica. PV was a key parameter for characterizing polar vortex. The PSC developed in the vortex may result in significant ODE by activating halogen species. To also assess changes after ozone recovery, we evaluated the PV, temperature, and ozone VCD from ground-based observations between March 18 and April 28, 2020 (Fig. 8).

205 Figure 8a–c shows that the tendencies for PV and ozone VCD are inversely related, i.e., PV correlates negatively with ozone VCD. Similarly, Arctic spring ozone depletion was closely related to PV. When ozone VCD decreased, the PV value increased. The ozone VCDs fluctuated between 241.2–334.6 DU, with ozone recovering to 388.1 DU on April 19, and then returning to normal values (Fig. 8a). The observed ozone VCD and temperature had similar fluctuation patterns, suggesting that ozone was significantly depleted in the colder Arctic low stratospheric vortex. Thus, the effect of the polar vortex on
210 ozone depletion in the stratosphere was clear.

3.3 Impact of halogen species

To further research the conditions and mechanisms of this ODE, we used a chemical model to characterize chemical components between November 1, 2019, and July 1, 2020. To validate the reliability of the WACCM simulated results, we needed to prove its capability for recreating observations in the atmosphere. Therefore, we compared WACCM simulations
215 with ozonesonde measurements. Figure 9 presents the comparison of temperature and ozone profiles over Ny-Ålesund from the WACCM simulations and the ozonesonde between January 1 and July 1, 2020. Fig. 9a–b shows a gradual depletion of ozone from 16 to 20 km in early March, and the mixing ratio at a similar altitude was unusually low from late March to early April, which corresponded to ground-based observations. A mixing ratio of less than 0.5 ppmv within the altitude range suggested that ozone was nearly completely depleted. This low value was uncommon, as the ozone mixing ratio was above



220 0.5 ppmv over the Arctic during 2011 (Solomon et al., 2014). There was an aberrantly cold spring in 2020, with low temperatures lasting until mid-April (Fig. 9c–d). In January and February 2020, the temperature in the 15–25 km altitude range was lower than T_{nat} , providing favourable conditions for PSC formation. As shown in Fig. 9, accurate simulations of the ozone and temperature profiles strengthened the credibility of the WACCM results. However, there are some discrepancies that exist in the model and observations. Because of the overestimation of temperature, the catalytic cycles that
225 cause ozone depletion in PSCs are underestimated. Therefore, there was an overestimation of ozone by the model compared to the observations.

Between late December 2019 and January 2020, we observed abnormally increasing, high HNO_3 values above Ny-Ålesund (Fig. 10b), suggesting abundant PSC formations. In contrast, in January 2011, analogous but lower values were recorded (Manney et al., 2011). Between late January and early February 2020, HNO_3 changed abruptly from abnormally high values
230 to normal values, which indicated the abundant PSC activities of the period.

In the PSC, chlorine and bromine compounds are activated and the activated halogen species can cause ozone depletion. Figure 10d–i presents the average diurnal concentration changes of chlorine and bromine compounds above Ny-Ålesund during the ODE. Between mid-February and early March 2020, the ClO level intensively increased over Ny-Ålesund, whereas the concentrations of ClONO₂ and HCl were low. However, the HBr levels remained elevated, which did not occur
235 in the HCl pattern during the same period. The results showed apparent chlorine activation during the Arctic spring of 2020.

During polar springs, PSCs and aerosol particles are considered to be the main cause of halogen species activation in the atmosphere (Portmann et al., 1996; Tritscher et al., 2021). Chlorine was activated by ClONO₂ + HCl and this reaction improved up to 10 times when the temperature reduced by 2.3 K (Wegner et al., 2012). Therefore, the persistently low temperatures during the Arctic spring of 2020 had a profound impact on the dominant chlorine activation reaction. In early
240 March, chlorine was deactivated as HCl, and the PSC that permitted chlorine activation remained. Activated chlorine compounds were mainly deactivated as ClONO₂ by the ClO + NO₂ reaction (Müller et al., 1994; Douglass et al., 1995). The model additionally simulated concentration changes in ClONO₂ from early March to mid-April 2020. In mid-April 2020, ClONO₂ stopped increasing and ClO was almost depleted when the ozone concentration started to recover. Chlorine activation began in early December 2019 as well as lasting until early April 2020. Owing to severe ozone depletion, large



245 amounts of HCl were produced during late March and April 2020, with an apparent HCl increase in mid-April, which was similar to the deactivation that occurred in the Antarctic.

Figure 11 displays the simulated average diurnal mixing ratios of ozone, chlorine, and bromine compounds for heights of 17.5 km above Ny-Ålesund, where significant ozone depletion occurred. Bromine was predominantly present as HOBr and BrONO₂ at night before chlorine activation, and almost all bromine was present as BrCl at night after chlorine activation in
250 the Arctic winter of 2004–2005 (Wohlmann et al., 2017). We also noted that the partitioning of bromine compounds differed from that of chlorine. HCl and ClONO₂ were the main constituents of Cl_t (the total concentration of the following chlorine compounds: ClO, HCl, HOCl, and ClONO₂) from November 2019 to late January 2020, whereas HOBr and BrCl were the main constituents of Br_t (the total concentration of the following bromine compounds: BrO, HBr, HOBr, BrONO₂, and BrCl) during the same period. BrCl was produced by the BrO + ClO reaction. Additionally, reactions in this period via
255 HOBr + hv into Br and via BrCl + hv into Br and Cl are extremely important for the contribution of both chlorine and bromine radicals. Consequently, the heterogeneous reaction of stratospheric Br increases the concentration of the active BrO component in the stratosphere. In February 2020, the values of HBr, HOBr and BrONO₂ in the simulated data set (Fig. 11b) were extremely low, while the BrO value started to increase.

Bromine existed mainly as HOBr before chlorine activation began. When chlorine was activated, BrCl became the major
260 constituent of Br_t. Because they rapidly photolyzed to Br in the daytime, these were not true reservoir gases compared with the lower active chlorine. Although the concentrations of these gases were quite low, there was a significant potential for ozone depletion (Lary, 1996; Solomon, 1999). BrO increased to its peak values on April 31, 2020, when ozone dropped to 1.16 ppmv. After April 18, BrO gradually stabilized and ozone began to recover, when the BrONO₂ produced by the BrO + NO₂ reaction became the main constituent of Br_t.

265 4 Conclusion

In this research, the ozone VCD was obtained from a ground-based instrument, the GOME-2 satellite, and the Brewer and SAOZ instruments and further evaluated with a correlation analysis. The Pearson correlation coefficients were 0.94, 0.86, and 0.91, and the relative deviations were 2.3%, 3.1%, and 3.5%, respectively. Therefore, we can conclude that the method



of observing the VCDs of Arctic ozone using a ground-based DOAS instrument is reliable and valid. In 2020, the daily peak
270 relative ozone losses compared to normal years from the GOME-2, ZSL-DOAS, Brewer, and SAOZ datasets were 43.6%,
44.3%, 40.3%, and 40.6%, respectively. The results indicated that all instruments recorded severe ozone depletion from
March 18 to April 18, 2020.

The effect of the polar vortex on ozone depletion in the stratosphere was clear. During the winter of 2019/2020, Arctic low
stratospheric temperatures were unusually low. The vortex was peculiarly steady before early April, enabling the PSCs to be
275 produced, and this matched the changes in simulated HNO_3 . This resulted in substantial ozone depletion until mid-April. The
observed ozone VCD and temperatures had similar fluctuation patterns, whereas PV was negatively correlated with ozone
VCD over Ny-Ålesund in the spring.

The ozone and temperature profiles were simulated by SD-WACCM, and these simulations corresponded well with
ozonesonde measurements. The model results show that ozone depletion at a height range of 16–20 km is evident from late
280 March to early April, which corresponds to the ozone VCDs obtained from the ground-based instrument. In 2020,
exceptional meteorological conditions contributed to a significant increase in reactive chlorine, resulting in an unprecedented
ozone loss in the Arctic. An apparent HCl increase occurred in mid-April 2020, when ClONO_2 stopped increasing and ClO
was almost depleted as the ozone concentration started to recover. Before chlorine activation began, bromine mainly existed
as HOBr; however, after chlorine activation, bromine mainly existed in the form of BrCl. Furthermore, they rapidly
285 photolyzed to Br in the daytime and had high potential to cause ozone depletion.

Observations of ozone VCDs over Ny-Ålesund will continue in order to monitor future ozone changes over the area. Further
synthetic analyses based on chemistry–climatic modeling and observational data are needed to study ozone recovery and its
effect on climate change and the ecological environment.

Data availability. Measurements and calculation of ozone VCDs above Ny-Ålesund, Norway, from 2017 to 2021 and the
290 results from the SD-WACCM used in this research are available from Yuhan Luo from AIOFM, CAS (yhluo@aiofm.ac.cn).
GOME-2 data are download from <https://avdc.gsfc.nasa.gov/>, Brewer data from <https://woudc.org/>, SAOZ data from



<http://saoz.obs.uvsq.fr/>, ECMWF data from <https://cds.climate.copernicus.eu/>, and ozonesonde data from <https://ndaccdemo.org/>.

Author contribution. QL: Methodology, Investigation, Software, Formal analysis, Validation, Visualization, Writing. YL:
295 Funding acquisition, Methodology, Formal analysis, Writing, Reviewing, Editing, Resources. YQ: Methodology, Software,
Formal analysis, Visualization. CP: Methodology, Software, Formal analysis. KD: Validation, Resources. XH: Methodology,
Formal analysis. FS: Validation, Resources. WL: Supervision.

Competing interests. The authors declare that they have no conflict of interest.

Acknowledgement. This research was financially supported by the National Natural Science Foundation of China (Grant
300 Nos.41941011 and 41676184) and the Youth Innovation Promotion Association of CAS (Grant No.2020439). We thank the
organizations of the Chinese Arctic and Antarctic Administration (CAAA), Polar Research Institute of China, and teammates
of the Chinese Arctic Yellow River Station for their kind help. We gratefully thank the BIRA for providing the QDOAS
software. The GOME-2 data can be available from the University of Bremen. The Brewer data can be provided by the World
Ozone and Ultraviolet Radiation Data Centre. We appreciate Florence Goutail for providing the SAOZ data. We gratefully
305 thank the Alfred Wegener Institute for providing ozonesonde data. We also gratefully thank ECMWF for providing the
ERA5 data.

References

- Arblaster, J. M., Gillett, N. P., Calvo, N., Forster, P., Polvani, L., Son, W., Waugh, D., Young, P., Barnes, E., and Cionni, I.:
Stratospheric ozone changes and climate, in: Scientific assessment of ozone depletion: 2014, World Meteorological
310 Organization, 2014.
- Bhartia, P. K.: OMI Algorithm Theoretical Basis Document Volume II, OMI Ozone, 2002.
- Bognar, K., Alwarda, R., Strong, K., Chipperfield, M. P., Dhomse, S. S., Drummond, J. R., Feng, W., Fioletov, V., Goutail,
F., and Herrera, B.: Unprecedented spring 2020 ozone depletion in the context of 20 years of measurements at Eureka,



- 315 Canada, *Journal of Geophysical Research: Atmospheres.*, 126, e2020JD034365, <https://doi.org/10.1029/2020JD034365>, 2021.
- Bogumil, K., Orphal, J., Homann, T., Voigt, S., Spietz, P., Fleischmann, O., Vogel, A., Hartmann, M., Kromminga, H., and Bovensmann, H.: Measurements of molecular absorption spectra with the SCIAMACHY pre-flight model: instrument characterization and reference data for atmospheric remote-sensing in the 230–2380 nm region, *Journal of Photochemistry and Photobiology A: Chemistry.*, 157, 167–184, [https://doi.org/10.1016/S1010-6030\(03\)00062-5](https://doi.org/10.1016/S1010-6030(03)00062-5), 2003.
- 320 Dameris, M., Loyola, D. G., Nützel, M., Coldewey-Egbers, M., Lerot, C., Romahn, F., and Van Roozendael, M.: Record low ozone values over the Arctic in boreal spring 2020, *Atmospheric Chemistry and Physics.*, 21, 617–633, <https://doi.org/10.5194/acp-21-617-2021>, 2021.
- Dameris, M.: Climate change and atmospheric chemistry: how will the stratospheric ozone layer develop?, *Angew Chem Int Ed Engl.*, 49, 8092–8102, <https://doi.org/10.1002/anie.201001643>, 2010.
- 325 Douglass, A. R., Schoeberl, M. R., Stolarski, R. S., Waters, J., Russell III, J. M., Roche, A. E., and Massie, S. T.: Interhemispheric differences in springtime production of HCl and ClONO₂ in the polar vortices, *Journal of Geophysical Research: Atmospheres.*, 100, 13967–13978, <https://doi.org/10.1029/95JD00698>, 1995.
- Farman, J.C., Gardiner, B.G., Shanklin, J.D.: Large losses of total ozone in Antarctica reveal seasonal ClO_x/NO_x interaction, *Nature.*, 315, 207–10, <https://doi.org/10.1038/315207a0>, 1985.
- 330 Frieß, U., Kreher, K., Johnston, P., and Platt, U.: Ground-based DOAS measurements of stratospheric trace gases at two Antarctic stations during the 2002 ozone hole period, *Journal of the atmospheric sciences.*, 62, 765–777, <https://doi.org/10.1175/JAS-3319.1>, 2005.
- Frieß, U., Kreher, K., Johnston, P.V., Platt, U.: Ground-based DOAS measurements of stratospheric trace gases at two Antarctic stations during the 2002 ozone hole period, *J. Atmos. Sci.*, 62, 765–77, <https://doi.org/10.1175/JAS-3319.1>, 2005.
- 335 Gelaro, R., McCarty, W., Suárez, M. J., Todling, R., Molod, A., Takacs, L., Randles, C. A., Darmenov, A., Bosilovich, M. G., and Reichle, R.: The modern-era retrospective analysis for research and applications, version 2 (MERRA-2), *Journal of climate.*, 30, 5419–5454, <https://doi.org/10.1175/JCLI-D-16-0758.1>, 2017.
- Groß, J.-U. and Müller, R.: Simulation of record Arctic stratospheric ozone depletion in 2020, *Journal of Geophysical Research: Atmospheres.*, 126, e2020JD033339, <https://doi.org/10.1029/2020JD033339>, 2021.
- 340 Groß, J.-U., Brauttsch, K., Pommrich, R., Solomon, S., & Müller, R.: Stratospheric ozone chemistry in the Antarctic: What controls the lowest values that can be reached and their recovery?, *Atmospheric Chemistry and Physics.*, 11, 12217–12226, <https://doi.org/10.5194/acp-11-12217-2011>, 2011.
- Groß, J.-U., Müller, R., Spang, R., Tritscher, I., Wegner, T., Chipperfield, M. P., Feng, W., Kinnison, D. E., and Madronich, S.: On the discrepancy of HCl processing in the core of the wintertime polar vortices, *Atmospheric Chemistry and Physics.*, 18, 8647–8666, <https://doi.org/10.5194/acp-18-8647-2018>, 2018.
- 345



- Hansen, G. and Chipperfield, M. P.: Ozone depletion at the edge of the Arctic polar vortex 1996/1997, *Journal of Geophysical Research: Atmospheres.*, 104, 1837-1845, <https://doi.org/10.1029/1998jd100021>, 1999.
- Harris, N., Lehmann, R., Rex, M., and von der Gathen, P.: A closer look at Arctic ozone loss and polar stratospheric clouds, *Atmospheric chemistry and physics.*, 10, 8499-8510, <http://doi:10.5194/acp-10-8499-2010>, 2010.
- Hermans, C., Vandaele, A., Fally, S., Carleer, M., Colin, R., Coquart, B., Jenouvrier, A., and Merienne, M. F.: Absorption cross-section of the collision-induced bands of oxygen from the UV to the NIR, in: *Weakly interacting molecular pairs: unconventional absorbers of radiation in the atmosphere*, Springer., 193-202, https://doi.org/10.1007/978-94-010-0025-3_16, 2003.
- Hu, Y.: The very unusual polar stratosphere in 2019–2020, *Science Bulletin.*, 65, 1775-1777, <https://doi.org/10.1016/j.scib.2020.07.011>, 2020.
- Kerr, J.: New methodology for deriving total ozone and other atmospheric variables from Brewer spectrophotometer direct sun spectra, *Journal of Geophysical Research: Atmospheres.*, 107, 4731, <https://doi.org/10.1029/2001JD001227>, 2002.
- Koukoulis, M. E., Clarisse, L., Carboni, E., van Gent, J., Spinetti, C., Balis, D., Dimopoulos, S., Grainger, D., Theys, N., and Tampellini, L.: Intercomparison of Metop-A SO₂ measurements during the 2010-2011 Icelandic eruptions, *Annals of Geophysics.*, 57, 2110, <https://doi.org/10.4401/ag-6613>, 2014.
- Kunz, A., Pan, L., Konopka, P., Kinnison, D., and Tilmes, S.: Chemical and dynamical discontinuity at the extratropical tropopause based on START08 and WACCM analyses, *Journal of Geophysical Research: Atmospheres.*, 116, D24302, <https://doi.org/10.1029/2011JD016686>, 2011.
- Kuttippurath, J., Godin-Beekmann, S., Lefèvre, F., Nikulin, G., Santee, M., and Froidevaux, L.: Record-breaking ozone loss in the Arctic winter 2010/2011: comparison with 1996/1997, *Atmospheric Chemistry and Physics.*, 12, 7073-7085, <https://doi.org/10.5194/acp-12-7073-2012>, 2012.
- Lamarque, J.-F., Emmons, L., Hess, P., Kinnison, D. E., Tilmes, S., Vitt, F., Heald, C., Holland, E. A., Lauritzen, P., and Neu, J.: CAM-chem: Description and evaluation of interactive atmospheric chemistry in the Community Earth System Model, *Geoscientific Model Development.*, 5, 369-411, <https://doi.org/10.5194/gmd-5-369-2012>, 2012.
- Lary, D.: Gas phase atmospheric bromine photochemistry, *Journal of Geophysical Research: Atmospheres.*, 101, 1505-1516, <https://doi.org/10.1029/95JD02463>, 1996.
- Lawrence, Z. D., Perlwitz, J., Butler, A. H., Manney, G. L., Newman, P. A., Lee, S. H., and Nash, E. R.: The remarkably strong Arctic stratospheric polar vortex of winter 2020: Links to record-breaking Arctic oscillation and ozone loss, *Journal of Geophysical Research: Atmospheres.*, 125, e2020JD033271, <https://doi.org/10.1029/2020JD033271>, 2020.
- Lu, L., Bian, L., and Xiao, C.: A study on polar atmospheric sciences and global change, *J Appl Meteorol Sci.*, 17, 743-755, 2006.
- Manney, G. L., Froidevaux, L., Santee, M. L., Livesey, N. J., Sabutis, J. L., and Waters, J. W.: Variability of ozone loss during Arctic winter (1991–2000) estimated from UARS Microwave Limb Sounder measurements, *Journal of Geophysical Research: Atmospheres.*, 108, 4149, <https://doi:10.1029/2002JD002634>, 2003.



- 385 Manney, G. L., Santee, M. L., Rex, M., Livesey, N. J., Pitts, M. C., Veefkind, P., Nash, E. R., Wohltmann, I., Lehmann, R., Froidevaux, L., Poole, L. R., Schoeberl, M. R., Haffner, D. P., Davies, J., Dorokhov, V., Gernandt, H., Johnson, B., Kivi, R., Kyro, E., Larsen, N., Levelt, P. F., Makshtas, A., McElroy, C. T., Nakajima, H., Parrondo, M. C., Tarasick, D. W., von der Gathen, P., Walker, K. A., and Zinoviev, N. S.: Unprecedented Arctic ozone loss in 2011, *Nature.*, 478, 469-475, <https://doi.org/10.1038/nature10556>, 2011.
- Manney, G. L., Livesey, N. J., Santee, M. L., Froidevaux, L., Lambert, A., Lawrence, Z. D., Millán, L. F., Neu, J. L., Read, W. G., and Schwartz, M. J.: Record-low Arctic stratospheric ozone in 2020: MLS observations of chemical processes and comparisons with previous extreme winters, *Geophysical Research Letters.*, 47, e2020GL089063, <https://doi.org/10.1029/2020GL089063>, 2020.
- 390 Marsing, A., Jurkat-Witschas, T., Groöß, J.-U., Kaufmann, S., Heller, R., Engel, A., Hoor, P., Krause, J., and Voigt, C.: Chlorine partitioning in the lowermost Arctic vortex during the cold winter 2015/2016, *Atmospheric Chemistry and Physics.*, 19, 10757-10772, <https://doi.org/10.5194/acp-19-10757-2019>, 2019.
- McElroy, M. B., Salawitch, R. J., Wofsy, S. C., & Logan, J. A.: Reductions of Antarctic ozone due to synergistic interactions of chlorine and bromine, *Nature.*, 321, 759–762, <https://doi.org/10.1038/321759a0>, 1986.
- 395 McKenna, D. S., Groöß, J.-U., Günther, G., Konopka, P., Müller, R., Carver, G., & Sasano, Y.: A new Chemical Lagrangian Model of the Stratosphere (CLaMS): 2. Formulation of chemistry scheme and initialization, *Journal of Geophysical Research.*, 107, 4256, <https://doi.org/10.1029/2000JD000113>, 2002.
- McKenzie, R. L., Aucamp, P. J., Bais, A. F., Bjorn, L. O., Ilyas, M., and Madronich, S.: Ozone depletion and climate change: impacts on UV radiation, *Photoch Photobio Sci.*, 10, 182-198, <https://doi.org/10.1039/c0pp90034f>, 2011.
- 400 Molina, L. and Molina, M.: Production of chlorine oxide (Cl_2O_2) from the self-reaction of the chlorine oxide (ClO) radical, *Journal of Physical Chemistry.*, 91, 433-436, <https://doi.org/10.1021/j100286a035>, 1987.
- Müller, R., Peter, T., Crutzen, P., Oelhaf, H., Adrian, G., Clarmann, T. v., Wegner, A., Schmidt, U., and Lary, D.: Chlorine chemistry and the potential for ozone depletion in the Arctic stratosphere in the winter of 1991/92, *Geophysical research letters.*, 21, 1427-1430, <https://doi.org/10.1029/94GL00465>, 1994.
- 405 Neale, R. B., Richter, J., Park, S., Lauritzen, P. H., Vavrus, S. J., Rasch, P. J., and Zhang, M.: The mean climate of the Community Atmosphere Model (CAM4) in forced SST and fully coupled experiments, *Journal of Climate.*, 26, 5150-5168, <https://doi.org/10.1175/JCLI-D-12-00236.1>, 2013.
- Pan, C., Zhu, B., Gao, J., Hou, X., Kang, H., and Wang, D.: Quantifying Arctic lower stratospheric ozone sources in winter and spring, *Scientific reports.*, 8, 1-9, <https://doi.org/10.1038/s41598-018-27045-5>, 2018.
- 410 Pan, C., Zhu, B., Gao, J., Kang, H., and Zhu, T.: Quantitative identification of moisture sources over the Tibetan Plateau and the relationship between thermal forcing and moisture transport, *Climate Dynamics.*, 52, 181-196, <https://doi.org/10.1007/s00382-018-4130-6>, 2019.
- Platt, U., and Stutz, J.: *Differential Optical Absorption Spectroscopy: Principles and Applications*, Springer., 568 pp, <https://doi.org/10.1007/978-3-540-75776-4>, 2008.



- 415 Pommereau, J. P. and Goutail, F.: O₃ and NO₂ ground-based measurements by visible spectrometry during Arctic winter and spring 1988, *Geophysical Research Letters.*, 15, 891-894, <https://doi.org/10.1029/GL015i008p00891>, 1988.
- Portmann, R., Solomon, S., Garcia, R., Thomason, L., Poole, L., and McCormick, M.: Role of aerosol variations in anthropogenic ozone depletion in the polar regions, *Journal of Geophysical Research: Atmospheres.*, 101, 22991-23006, <https://doi.org/10.1029/96jd02608>, 1996.
- 420 Salawitch, R. J., Gobbi, G. P., Wofsy, S. C., & McElroy, M. B.: Denitrification in the Antarctic stratosphere, *Nature.*, 339, 525–527, <https://doi.org/10.1038/339525a0>, 1989.
- Simpson, W. R., Von Glasow, R., Riedel, K., Anderson, P., Ariya, P., Bottenheim, J., Burrows, J., Carpenter, L., Frieß, U., and Goodsite, M. E.: Halogens and their role in polar boundary-layer ozone depletion, *Atmospheric Chemistry and Physics.*, 7, 4375-4418, <https://doi.org/10.5194/acp-74375-2007>, 2007.
- 425 Solomon, S.: Stratospheric ozone depletion: A review of concepts and history, *Reviews of Geophysics.*, 37, 275-316, <https://doi.org/10.1029/1999RG900008>, 1999.
- Solomon, S., Portmann, R. W., and Thompson, D. W.: Contrasts between Antarctic and Arctic ozone depletion, *Proceedings of the National Academy of Sciences.*, 104, 445-449, <https://doi.org/10.1073/pnas.0604895104>, 2007.
- Solomon, S., Haskins, J., Ivy, D. J., and Min, F.: Fundamental differences between Arctic and Antarctic ozone depletion, *Proceedings of the National Academy of Sciences.*, 111, 6220-6225, <https://doi.org/10.1073/pnas.1319307111>, 2014.
- 430 Solomon, S., Ivy, D. J., Kinnison, D., Mills, M. J., Neely, R. R., and Schmidt, A.: Emergence of healing in the Antarctic ozone layer, *Science.*, 353, 269-274, <https://doi.org/10.1126/science.aae0061>, 2016.
- Toohey, D., Avallone, L., Lait, L., Newman, P., Schoeberl, M., Fahey, D., Woodbridge, E., and Anderson, J.: The seasonal evolution of reactive chlorine in the northern hemisphere stratosphere, *Science.*, 261, 1134-1136, <https://doi.org/10.1126/science.261.5125.1134>, 1993.
- 435 Tritscher, I., Pitts, M. C., Poole, L. R., Alexander, S. P., Cairo, F., Chipperfield, M. P., Groöß, J. U., Höpfner, M., Lambert, A., and Luo, B.: Polar stratospheric clouds: Satellite observations, processes, and role in ozone depletion, *Reviews of geophysics.*, 59, e2020RG000702, <https://doi.org/10.1029/2020RG000702>, 2021.
- Vandaele, A. C., Hermans, C., Simon, P. C., Van Roozendaal, M., Guilmot, J. M., Carleer, M., and Colin, R.: Fourier transform measurement of NO₂ absorption cross-section in the visible range at room temperature, *Journal of atmospheric chemistry.*, 25, 289-305, <https://doi.org/10.1007/BF00053797>, 1996.
- 440 Wegner, T., Groöß, J.-U., Von Hobe, M., Stroh, F., Sumińska-Ebersoldt, O., Volk, C., Hösen, E., Mitev, V., Shur, G., and Müller, R.: Heterogeneous chlorine activation on stratospheric aerosols and clouds in the Arctic polar vortex, *Atmospheric Chemistry and Physics.*, 12, 11095-11106, <https://doi.org/10.5194/acp-12-11095-2012>, 2012.
- 445 Wohltmann, I., Lehmann, R., and Rex, M.: A quantitative analysis of the reactions involved in stratospheric ozone depletion in the polar vortex core, *Atmospheric Chemistry and Physics.*, 17, 10535-10563, <https://doi.org/10.5194/acp-17-10535-2017>, 2017.



- 450 Wohltmann, I., von der Gathen, P., Lehmann, R., Maturilli, M., Deckelmann, H., Manney, G. L., Davies, J., Tarasick, D., Jepsen, N., and Kivi, R.: Near-complete local reduction of Arctic stratospheric ozone by severe chemical loss in spring 2020, *Geophysical Research Letters.*, 47, e2020GL089547, <https://doi.org/10.1029/2020GL089547>, 2020.
- Wohltmann, I., von der Gathen, P., Lehmann, R., Deckelmann, H., Manney, G., Davies, J., Tarasick, D., Jepsen, N., Kivi, R., and Lyall, N.: Chemical evolution of the exceptional Arctic stratospheric winter 2019/2020 compared to previous Arctic and Antarctic winters, *Journal of Geophysical Research: Atmospheres.*, 126, e2020JD034356, <https://doi.org/10.1029/2020JD034356>, 2021.
- 455 Zhao, X., Fioletov, V., Brohart, M., Savastiouk, V., Abboud, I., Ogyu, A., Davies, J., Sit, R., Lee, S. C., and Cede, A.: The world Brewer reference triad–updated performance assessment and new double triad, *Atmospheric Measurement Techniques.*, 14, 2261–2283, <https://doi.org/10.5194/amt-2020-324>, 2021.



Table 1. Fitting parameters of spectral retrieval.

Parameter	References
O ₃	223K, 243K (Bogumil et al., 2003)
O ₄	293K (Hermans et al., 2003)
Ring	Ring.exe
Fitting Interval	320–340 nm
Polynomial	5



Table 2. The fitting parameter nodes for spectral retrieval.

Parameters	Nodes
SAZ (°)	35, 40, 45, 50, 55, 60, 65, 70, 75, 80
Surface albedo	0.05, 0.1, 0.2, 0.3, 0.4, 0.5, 0.6
Wavelength (nm)	From 320 to 340 in 0.5 intervals



460 **Table 3. The number of days below T_{nat} and daily average temperatures (December–February).**

Date	Days below T_{nat}	Average temperature (K)
2016.12–2017.2	0	203.5
2017.12–2018.2	26	203.6
2018.12–2019.2	0	211.8
2019.12–2020.2	32	196.9
2020.12–2021.2	6	205.3

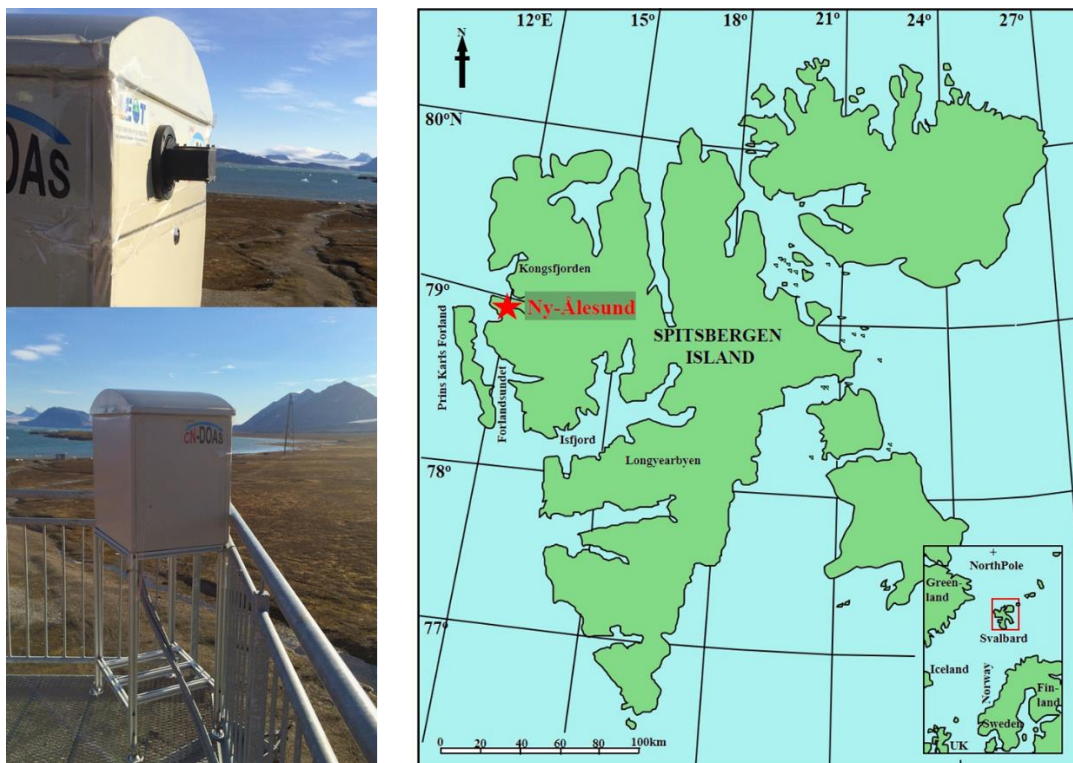


Figure 1. The ground-based ZSL-DOAS instrument and experiment site in Ny-Ålesund.

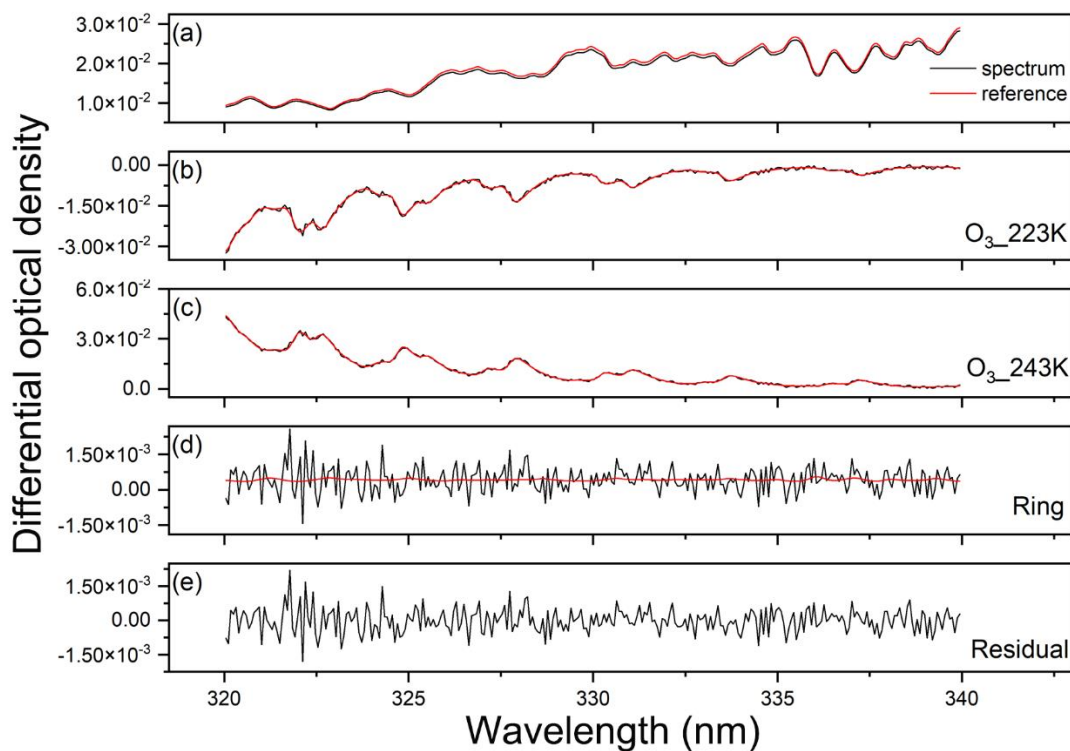
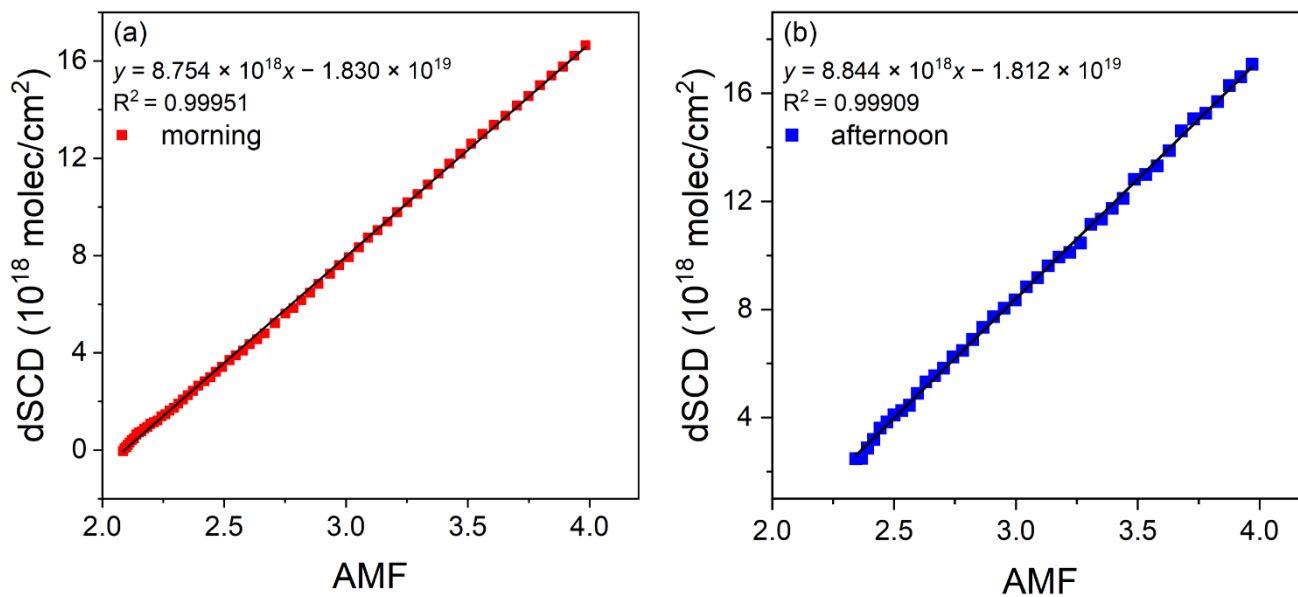
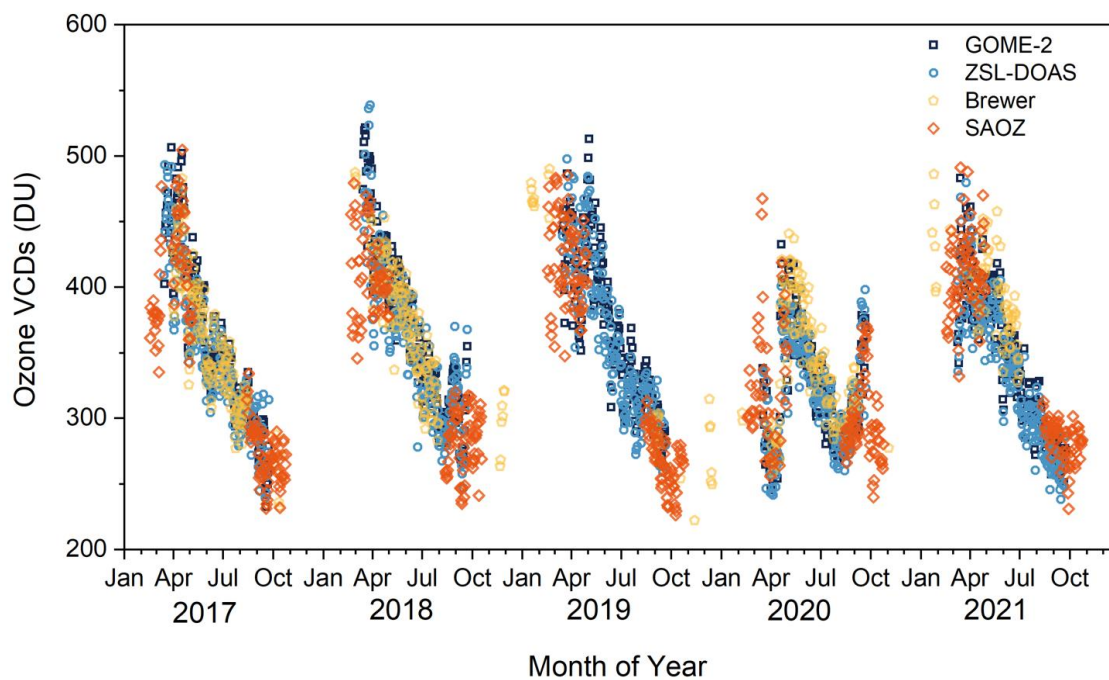


Figure 2. Spectrum fits of ozone on June 13, 2021.



465

Figure 3. Linear fit between ozone dSCDs and AMFs for the (a) morning and (b) afternoon on June 13, 2021. The correlation coefficients (R^2) are 0.99951 and 0.99909. The ozone VCDs for the morning and afternoon are 8.754×10^{18} molec cm^{-2} and 8.844×10^{18} molec cm^{-2} . The calculated ozone VCD for June 13, 2021 is 8.799×10^{18} molec cm^{-2} .



470 **Figure 4.** The ozone VCDs from ZSL-DOAS, GOME-2, Brewer, and SAOZ.

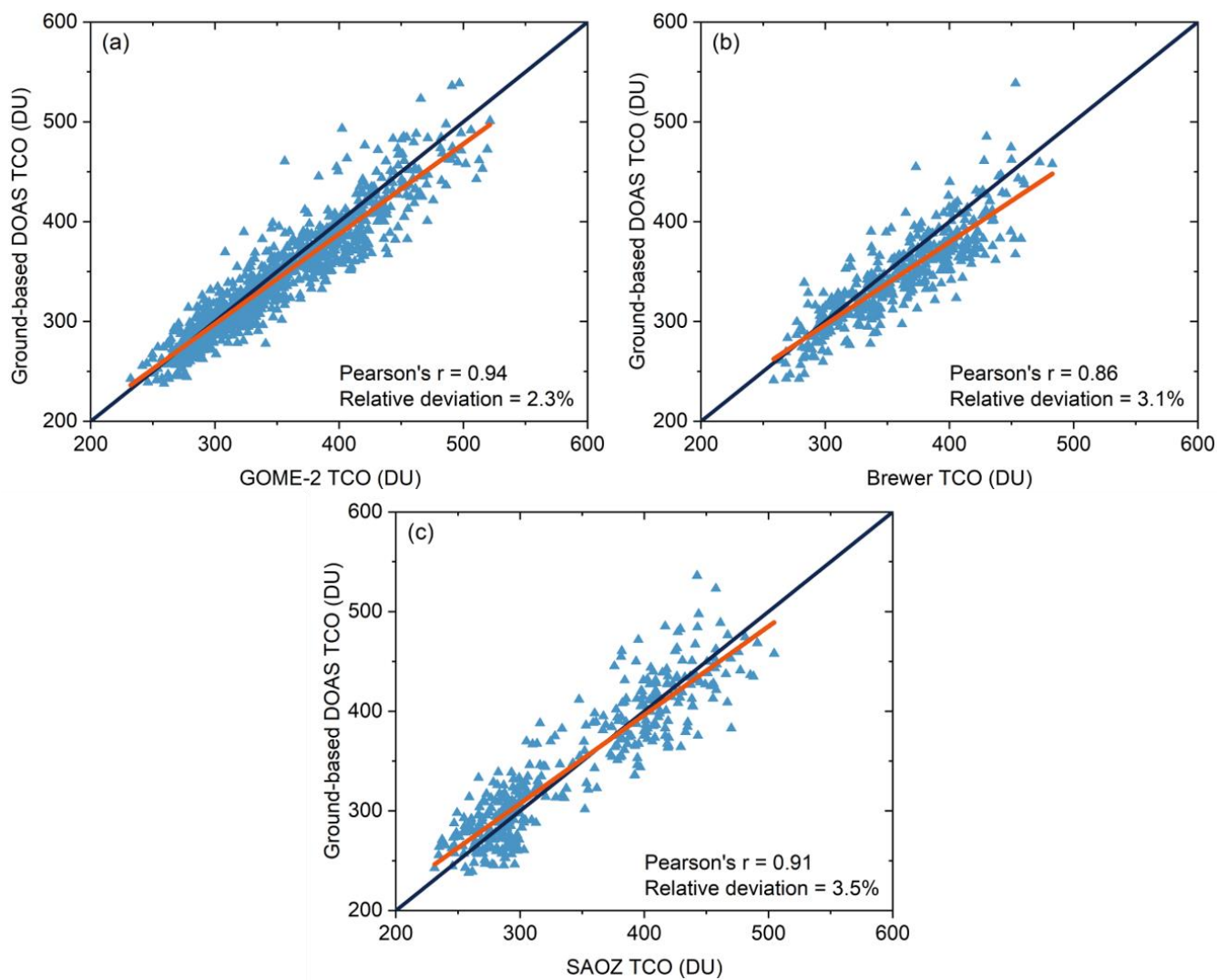


Figure 5. Scatter plots and linear fits of retrieved ozone VCDs with (a) GOME-2, (b) Brewer, and (c) SAOZ.

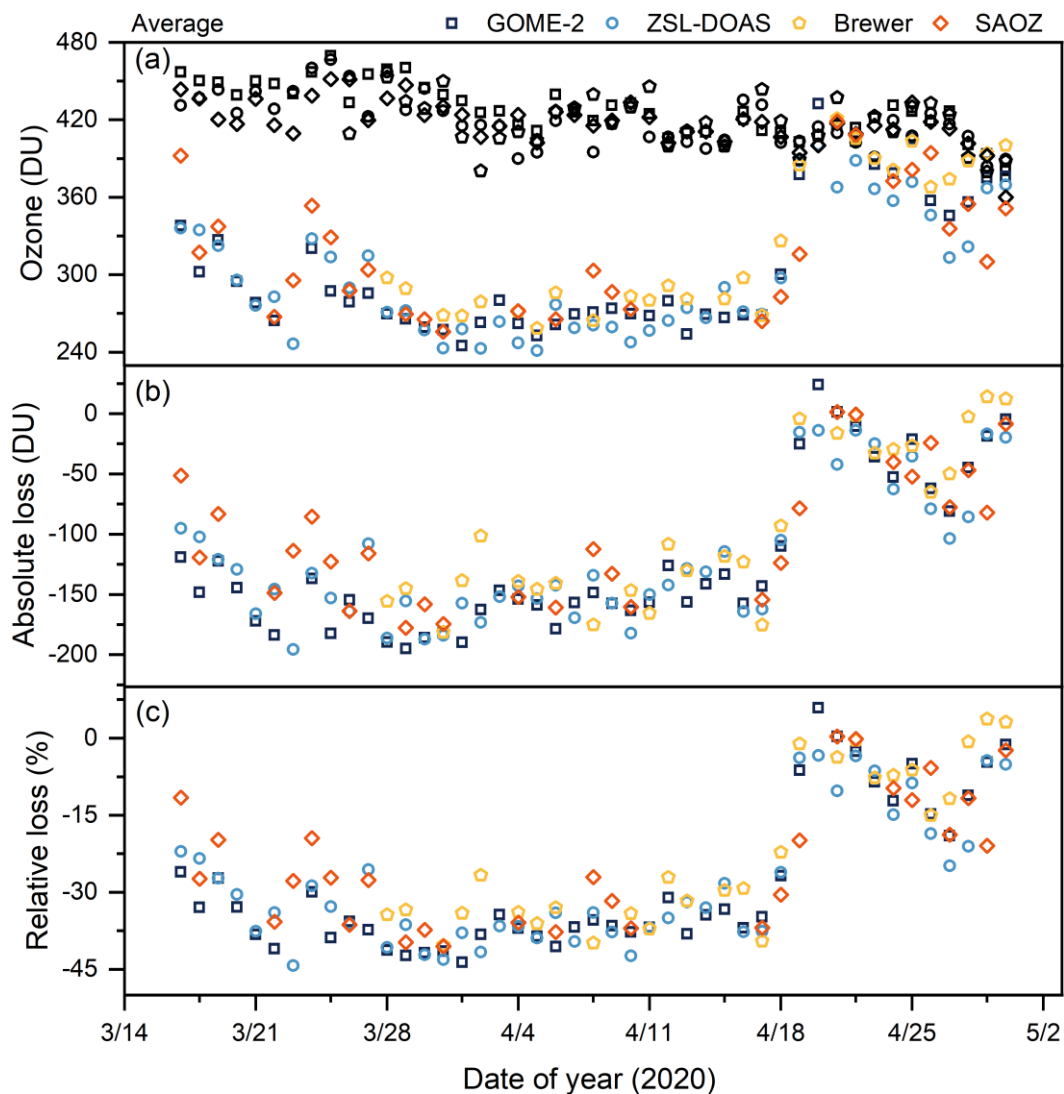


Figure 6. (a) Ozone data for 2020 and the average ozone data (black) of 2017, 2018, 2019, and 2021. (b) Absolute and (c) relative ozone loss for 2020.

475

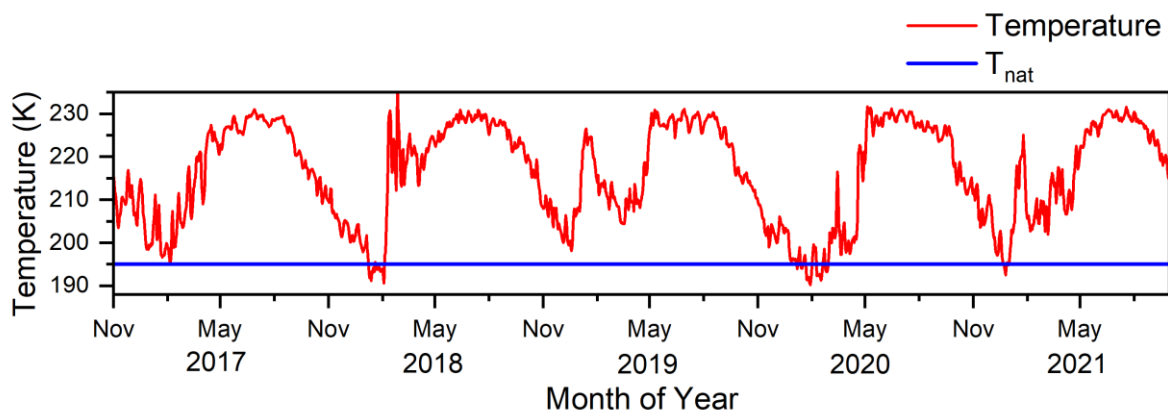
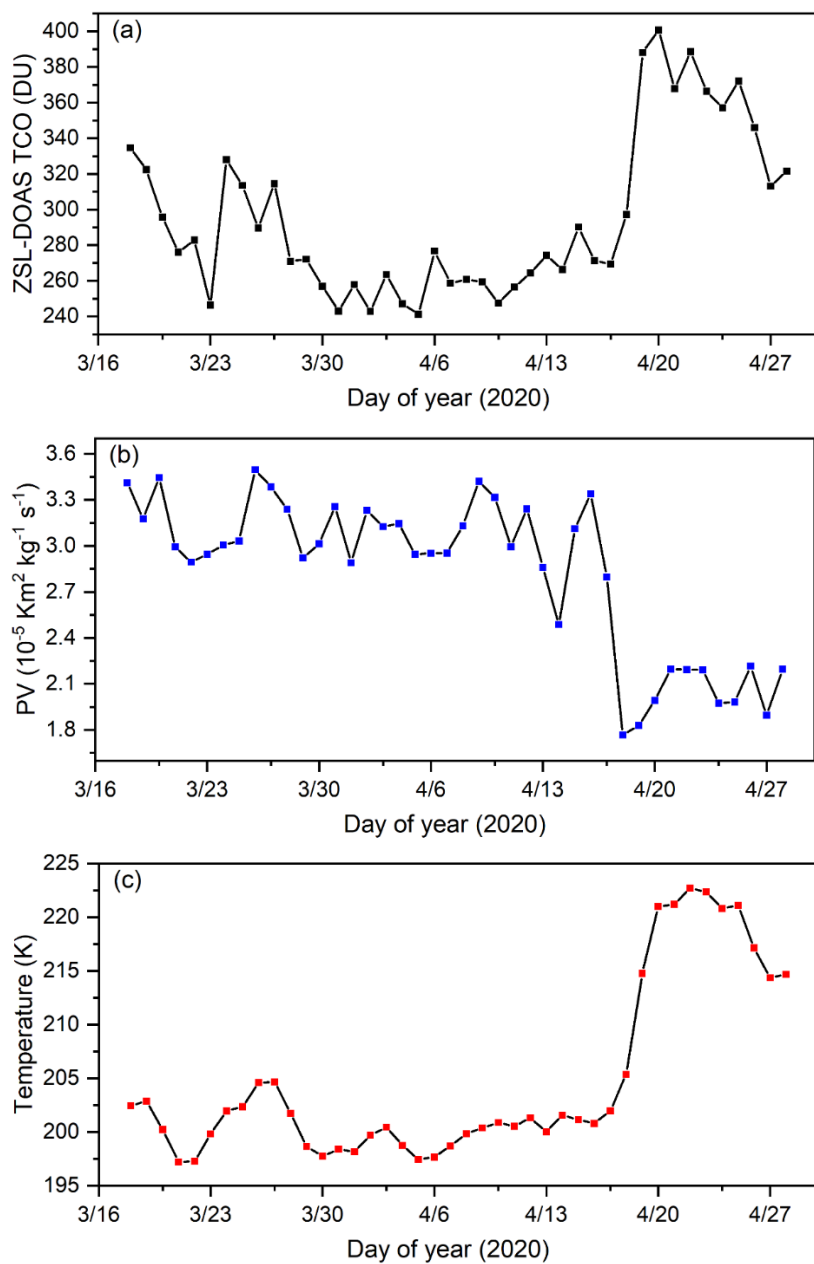


Figure 7. Temperatures (at 70 hPa) over Ny-Ålesund from November 2016 to September 2021, where the blue line denotes the threshold temperature for the formation of PSCs.



480 **Figure 8.** From March 18 to April 28, 2020: (a) retrieved ozone VCDs, (b) PVs (at 70 hPa), and (c) temperatures (at 70 hPa).

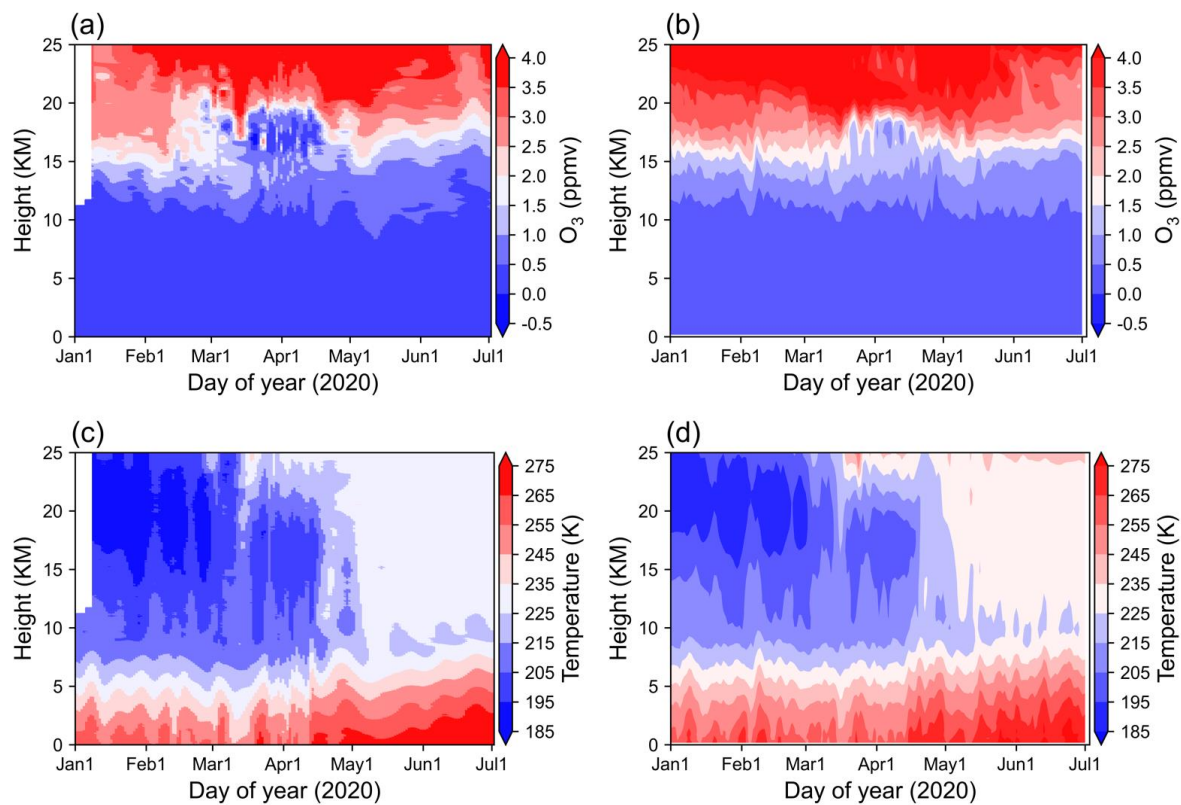
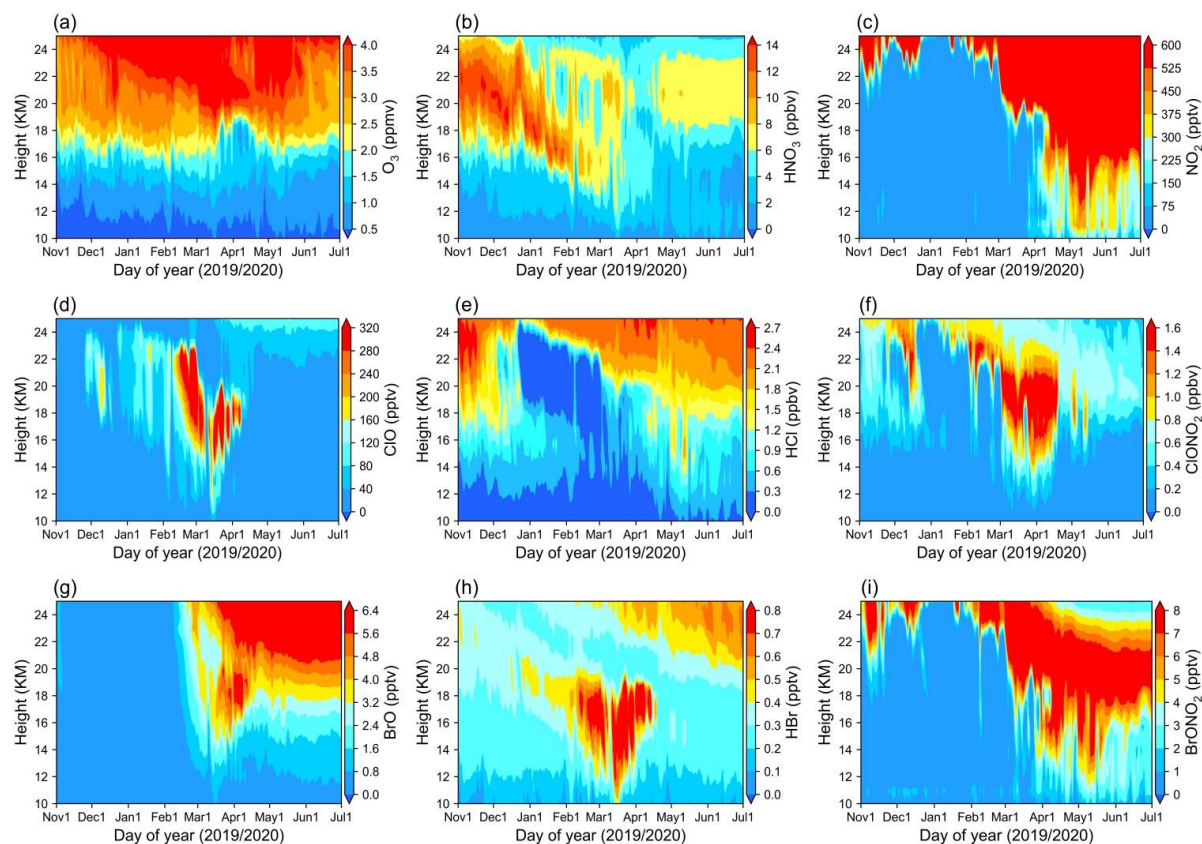
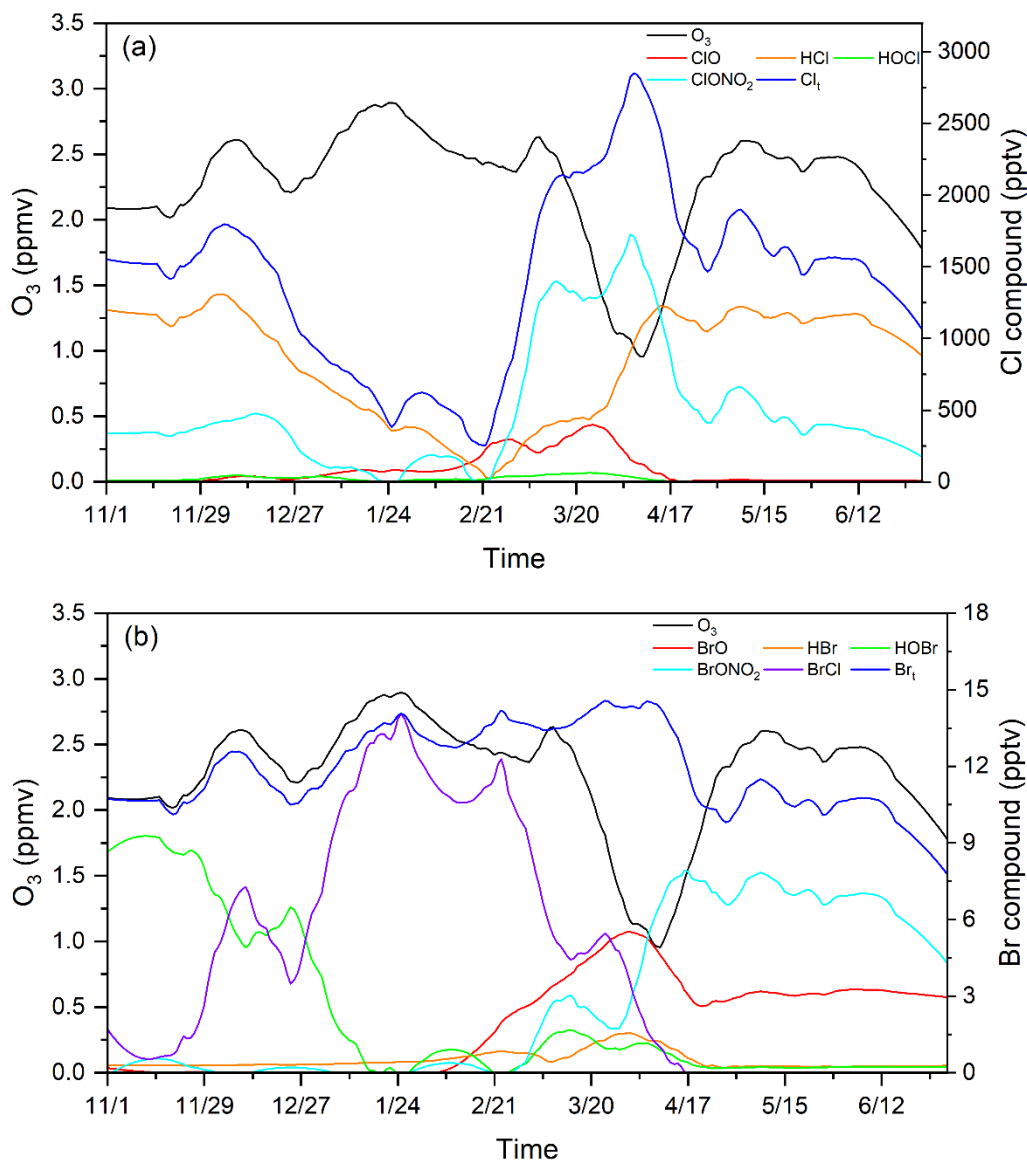


Figure 9. Between January 1 and July 1, 2020, ozone profiles from (a) ozonesonde measurements and (b) the WACCM simulation, and temperature profiles from (c) ozonesonde measurements and (d) the WACCM simulation.



485 **Figure 10.** Simulated average diurnal profiles of the chlorine and bromine compounds between November 1, 2019, and July 1, 2020, at heights of 10–25 km above Ny-Ålesund: (a) O₃; (b) HNO₃; (c) NO₂; (d) ClO; (e) HCl; (f) ClONO₂; (g) BrO; (h) HBr; (i) BrONO₂.



490 **Figure 11.** Simulated average diurnal mixing ratios of ozone, chlorine, and bromine compounds between November 1, 2019, and July 1, 2020, at a height of 17.5 km above Ny-Ålesund: (a) mixing ratios of ozone and chlorine ($Cl_t = ClO + HCl + HOCl + ClONO_2$); (b) mixing ratios of ozone and bromine ($Br_t = BrO + HBr + HOBr + BrONO_2 + BrCl$).